AIRCRAFT AND SHIP OBSERVATIONS OF THE MEAN STRUCTURE OF THE MARINE BOUNDARY LAYER OVER THE ARABIAN SEA DURING MONEX 79

T. HOLT and S. SETHURAMAN

Department of Marine, Earth and Atmospheric Sciences, North Carolina State University, Raleigh, NC 27695-8208, U.S.A.

(Received in final form 3 January, 1985)

Abstract. Analysis of the mean wind, equivalent potential temperature and virtual potential temperature profiles observed by the National Center for Atmospheric Research (NCAR) Electra aircraft and obtained from dropwindsondes and ship-launched radiosondes were made in conjunction with synoptic observations to study the structure of the monsoon boundary layer over the Arabian Sea during MONEX 79. Comparison of mean profiles indicates the monsoon boundary layer to be much different from the trade wind boundary layer. Results confirm the existence of a boundary-layer jet known as East African or Somali Jet. Regions of multiple cloud layers at roughly the height of the capping inversion layer were associated with the jet. Regions in which a more well-mixed layer was observed showed a jet structure depressed in height. A free-jet surface-layer model appears to describe the mean wind structure of this jet observed during the present study and by others. An approximate balance of forces was found in the monsoon boundary layer between friction, advective acceleration, Coriolis and pressure gradient forces. Friction and advective acceleration terms were significant in the lower levels of the boundary layer. Forces in a typical trade wind boundary layer were found to be approximately one order of magnitude smaller than those observed in the monsoon boundary layer.

1. Introduction

Structure of a monsoon boundary layer such as the Indian southwest monsoon is different from a trade wind boundary layer in several aspects, one of which is its generation. The driving force behind the establishment of the monsoon is different from forces involved in trade wind flow. The large-scale circulation inherent in the monsoon flow seems to affect the motions of the order of a few kilometers which is essentially a boundary-layer-type of scale. There are only limited numbers of observational sets of data available on the monsoon boundary layer. International Indian Ocean Expedition, Indo-Soviet Monsoon Experiment (ISMEX), MONSOON 77, and MONEX 79 have provided valuable boundary-layer data. Analysis of some of these data has indicated the monsoon boundary layer to be markedly different from the trade wind boundary layers. Typical mean vertical profiles of virtual potential temperature θ_v, specific humidity q and wind speed U for an undisturbed trade-wind boundary layer are shown in Figure 1. There is generally uniform distribution of temperature and humidity in the trade-wind boundary layer with a well-mixed layer up to a height of about 700 m and an essentially constant specific humidity profile in this layer. Winds are fairly weak with little vertical shear. However, the monsoon boundary layer is generally characterized by a much stronger moisture lapse rate and an increase of wind with height in the subcloud layer (Long, 1980). Within the inversion layer of the monsoon boundary layer, there could be even an increase in the moisture as compared to trade wind PBLs where a

Boundary Layer Meteorology 33 (1985) 259–282. 0006–8314/85.15.

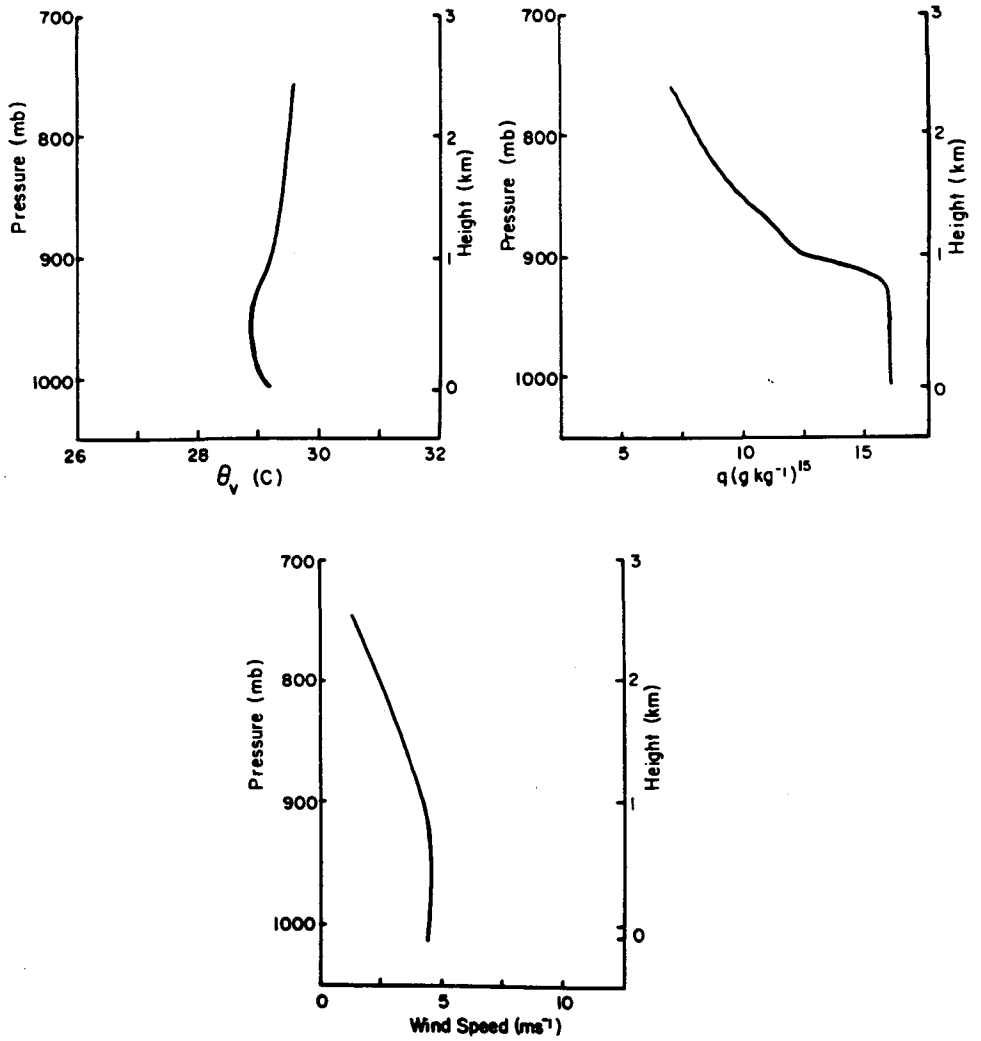

Fig. 1. Typical mean vertical profiles of virtual potential temperature θ_v, specific humidity q and wind speed for an undisturbed trade-wind boundary layer. Note the sharp decrease in specific humidity at the top of the boundary layer (about 925 mb). Wind speeds are constant throughout the mixed layer.

sharp decrease is generally observed. The purpose of this paper is to present observations on the mean structure of the marine boundary layer over the Arabian Sea characterized by the mean wind and temperature profiles obtained by research aircraft and ships during MONEX 79.

2. Large-Scale Features During Monsoons over the Arabian Sea

The Somali or East African Jet (EAJ) is an important feature of the summer monsoon low-level flow over the Arabian Sea. It is comprised of three main features (Bannon, 1982) – (a) southeast trades of the southern hemisphere, (b) strong cross-equatorial flow

off East Africa and western Indian Ocean, and (c) southwest monsoon flow over the Arabian Sea. Studies by Findlater (1977a) and van de Boogaard (1977) document the climatological structure of the jet. A schematic view of the EAJ over the Arabian Sea is given in Figure 2. Calculations by Findlater (1977a) show the jet accounting for

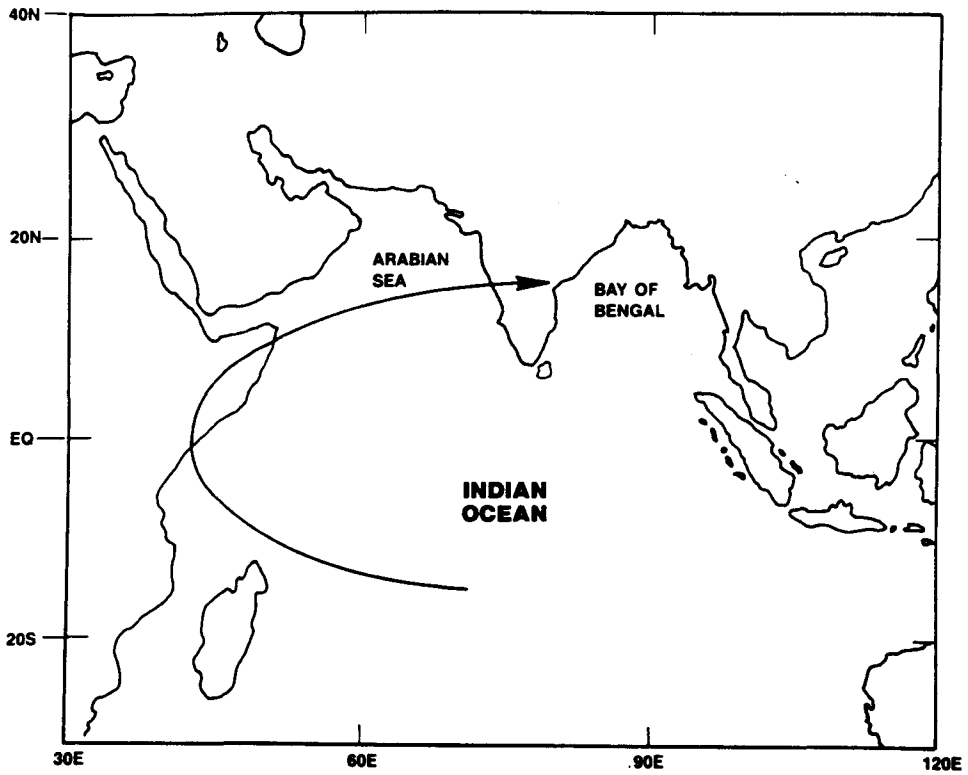

Fig. 2. Map of monsoon area showing the normally observed axis of the EAJ indicated by the arrow.

approximately one-half of all cross-equatorial transport of air in the lower troposphere in July. The southeast trades are generally from a more east-southeast direction with speeds on the order of 5–10 m s^{-1} with a relative maximum at approximately 17° S lat. As the jet crosses the equator with strong southerly flow, the core is situated at an altitude of 1.5 to 2.0 km with mean maximum speed of 15 m s^{-1} over East Africa. Usual separation from the African coast seems to occur at 10° N with wind speed maximum 20 m s^{-1} at about 1 km height to the northeast of the tip of the Horn of Somalia as shown in Figure 2. Mean sea level pressure distributions for July (van de Boogaard, 1977) show the Mascerene high pressure area dominating in the southern hemisphere with the equatorial trough conspicuously absent. In the northern hemisphere the monsoon trough extends across South Asia stretching down through central India. Orographic effects of the coastal mountains of East Africa seem to be important in intensifying the jet.

3. Synoptic conditions

Different stages of monsoon flow existed for the two NCAR Electra aircraft boundary-layer flight days, SEA1 (June 20, 1979) and SEA2 (June 24, 1979). Synoptic conditions for the period June 19–20, as seen in the June 20 sea level pressure field for 1200 GMT

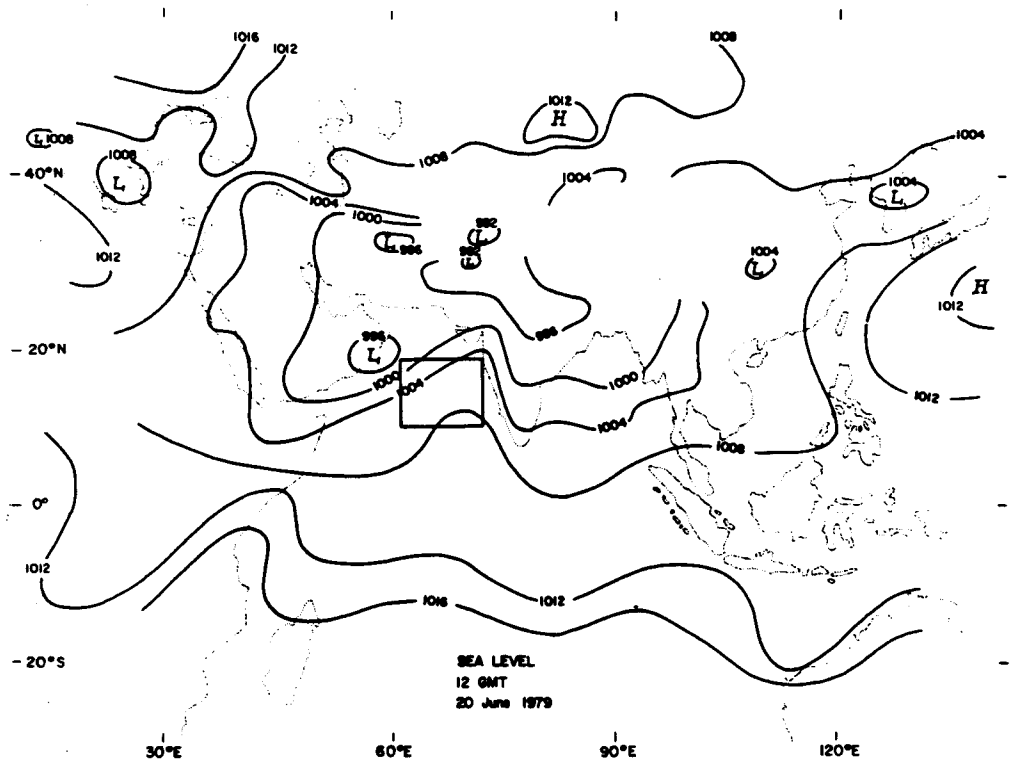

Fig. 3. Sea-level pressure field for 1200 GMT on June 20, 1979 showing the weakened tropical storm at 19° N, 57° E and the low-level southwesterly flow over the Arabian Sea. Box indicates area of boundary-layer observations.

(Figure 3), were indicative of the developing conditions for monsoon activity. The area of aircraft and ship observations in the boundary layer on June 20 is marked in Figure 3 by a box centered near 18° N, 65° E. Strong southwest monsoon low-level flow over the Arabian Sea was present on June 19 with strong upper-level easterlies. A weakened tropical storm was located at 19° N, 57° E near the Oman coast. By June 20 the tropical storm had almost dissipated; a low-level monsoon center was located over the Arabian Sea with strong convective activity and heavy rainfall along the western Indian coast and strong southwest flow up to 700 mb over the Arabian Sea. Synoptic conditions for the period June 23–25, 1979 showed well established monsoon conditions. Figure 4 shows the June 24 sea level pressure field for 1200 GMT with the box denoting the area of boundary-layer observations. Strong southwesterly flow was present over the Arabian Sea with a large monsoon depression at the head of the Bay of Bengal. A

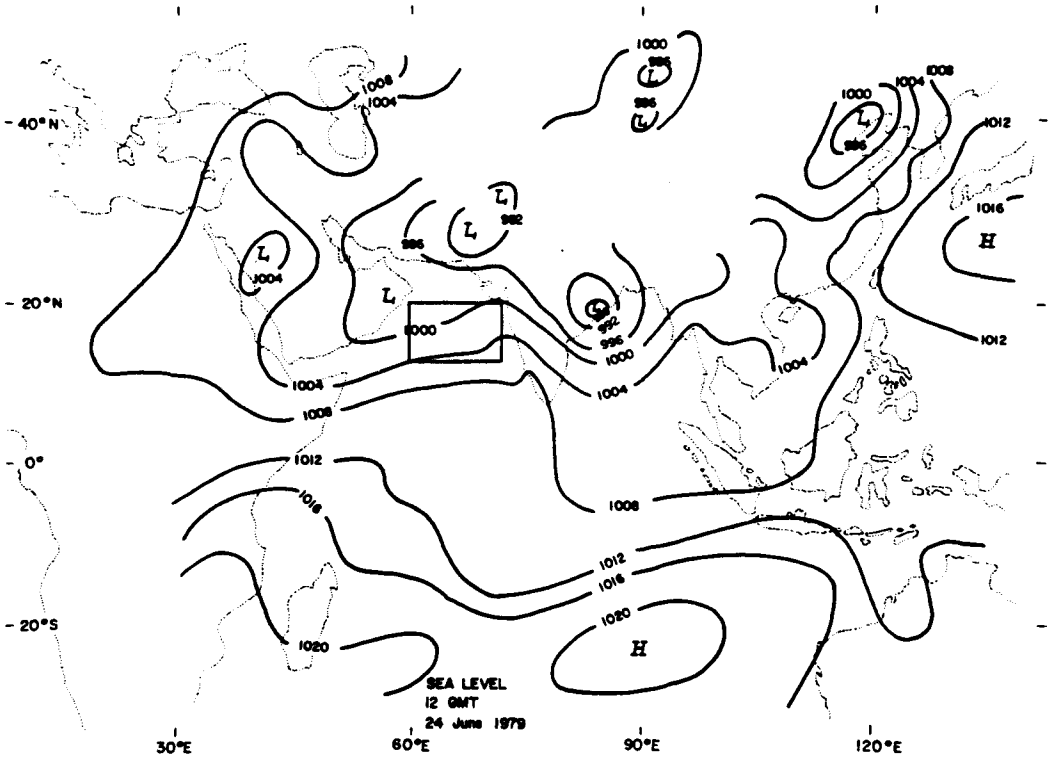

Fig. 4. Sea-level pressure field for 1200 GMT on June 24, 1979 showing the strong southwesterly flow over the Arabian Sea. Box indicates area of boundary-layer observations.

well-developed monsoon trough was present with most of India under massive cloudiness with strong convective activity along both coasts. By June 24 the monsoon was well established with southwest flow over the Arabian Sea and a 700 mb trough developing over it. Continued convection was present over the Bay associated with the trough. Strong upper-level easterly flow of 70 kt (36 m s^{-1}) was evident over the southern Indian tip. By June 25 the monsoon system still had strong southwest flow. The Bay of Bengal depression had moved inland to 22° N, 83° E with the trough stretching southwest to 15° N, 93° E. Rain activity was still heavy in central India due to the depression. A broad anticyclonic ridge was situated at 200 mb with strong low-level westerly flow at 850 mb (60 kt (31 m s^{-1}) at 15° N, 80° E). In summary, the synoptic pattern on June 20 can be considered as a developing monsoon flow and on June 24 as a developed monsoon. The strong southwesterly monsoon flow did not cover the entire Arabian Sea area until June 22 (Sikka and Grossman, 1980).

4. Data Analysis

Observations used in this paper consist of: (i) low-level flight data from the NCAR Electra research aircraft (ii) dropwindsonde observations from the NCAR Electra and

the NOAA P-3 aircraft, (iii) observations from ships (iv) synoptic weather observations, and (v) reports by observers on the aircraft.

Low-level flight data collected from the NCAR Electra aircraft consisted of high frequency (20 Hz) fluctuations of components of wind speed, ambient temperature and specific humidity for altitudes ranging from approximately 80 to 700 m. Details on the instrumentation of the Electra aircraft can be found in the Summer MONEX Field Phase Report (WMO, 1981). Altitude of the aircraft and latitude and longitude were also recorded. Flight tracks for the two observation days, June 20 and 24 are shown in Figures 5 and 6, respectively. Aircraft data used in this study were collected along the

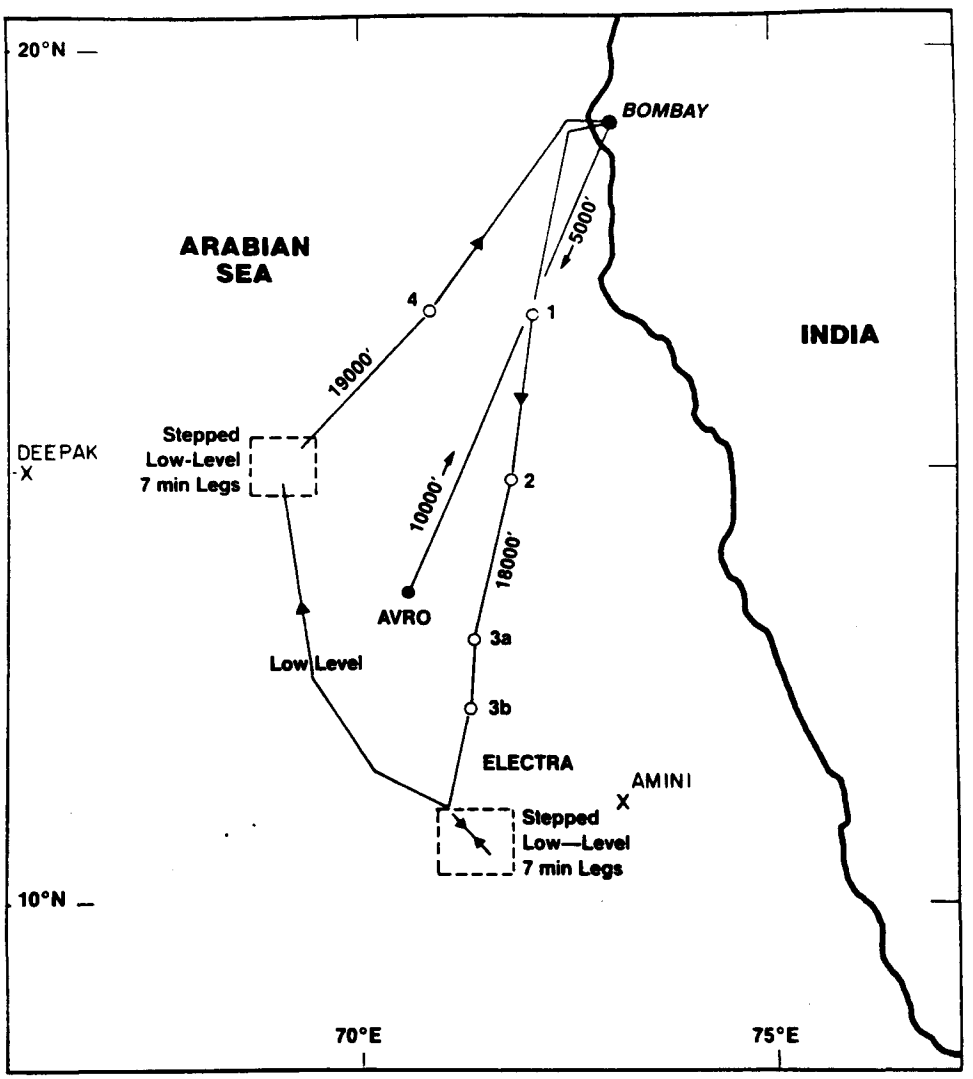

Fig. 5. Flight track for the NCAR Electra on June 20, 1979 over the Arabian Sea. Aircraft data for this study were collected along the low-level portion extending from 11° N to 15° N latitude. Open circles denote dropwindsondes. Location of MONEX ships DEEPAK and AMINI is also given. Boxes indicate area of low-level manoeuvers.

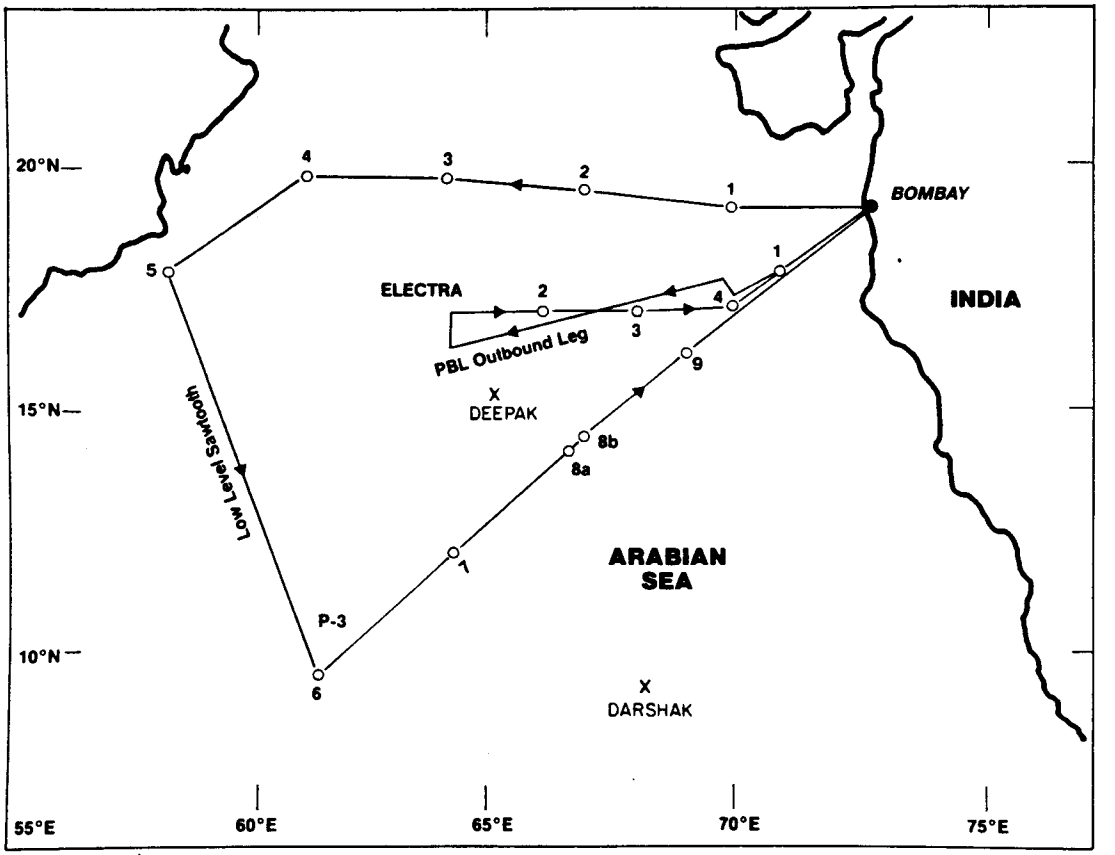

Fig. 6. Flight track for the NCAR Electra on June 24, 1979 over the Arabian Sea. Data were collected along the PBL outbound leg for this study. Track was generally into the surface wind. Location of MONEX ships DARSHAK and DEEPAK is given. Open circles denote dropwindsondes.

low-level portions of the flight track shown in Figure 5 and the PBL outbound leg portion of Figure 6. Ship positions are also provided. Cross-sections of the cloud structure obtained from aircraft observers' reports and satellite photos for the two days are shown in Figures 7 and 8. The cross-sections for both cases are along the flight tracks.

Ship data and dropwindsonde observations from the NCAR Electra provided pressure, temperature, dew point depression and wind speed as well as latitude and longitude. Synoptic weather maps provided information concerning the location and movement of large-scale systems affecting the boundary-layer processes.

Analysis involved computations of means and variances of each parameter for the three flight days for the latitude and longitude location. In this paper, mean wind, temperature and humidity variations in the vertical and horizontal planes are presented for the two days and their structures discussed.

5. Discussion of Results

As discussed above, one of the main features of the boundary-layer flow over the Arabian Sea is the existence of an elevated jet known as the East African Jet or Somali Jet. This is believed to be a result of the conservation of potential vorticity of air flowing across the equator due to the deflection of the easterly zonal flow by the East African mountains. Large-scale features of the jet have been studied observationally by Findlater (1969, 1977b) and with numerical models by Krishnamurti *et al.* (1976) among others. In this section, the structure of this jet over the Arabian Sea along with the temperature structure observed during MONEX 79 on June 20 and 24 will be discussed as well as the observations of the mean wind and temperature profiles for both the days.

Because of the direction of the NCAR Electra flight track and the differences in synoptic conditions, results for June 20 are divided into a Southern Arabian Sea region (approximate location 10.8° N, 71.2° E) and a Northern Arabian Sea region (14.8° N, 69.0° E); results for June 24 are divided into a Western Arabian Sea region (16.5° N, 63.9° E) and an Eastern Arabian Sea region (17.2° N, 69.9° E).

5.1. Mean Temperature and Wind Profiles

5.1.1. *June 20*

5.1.1.1. Southern Arabian Sea. Synoptic-scale cloud conditions over the Southern Arabian Sea on June 20 were obtained from ship data, NCAR Electra aircraft observers'

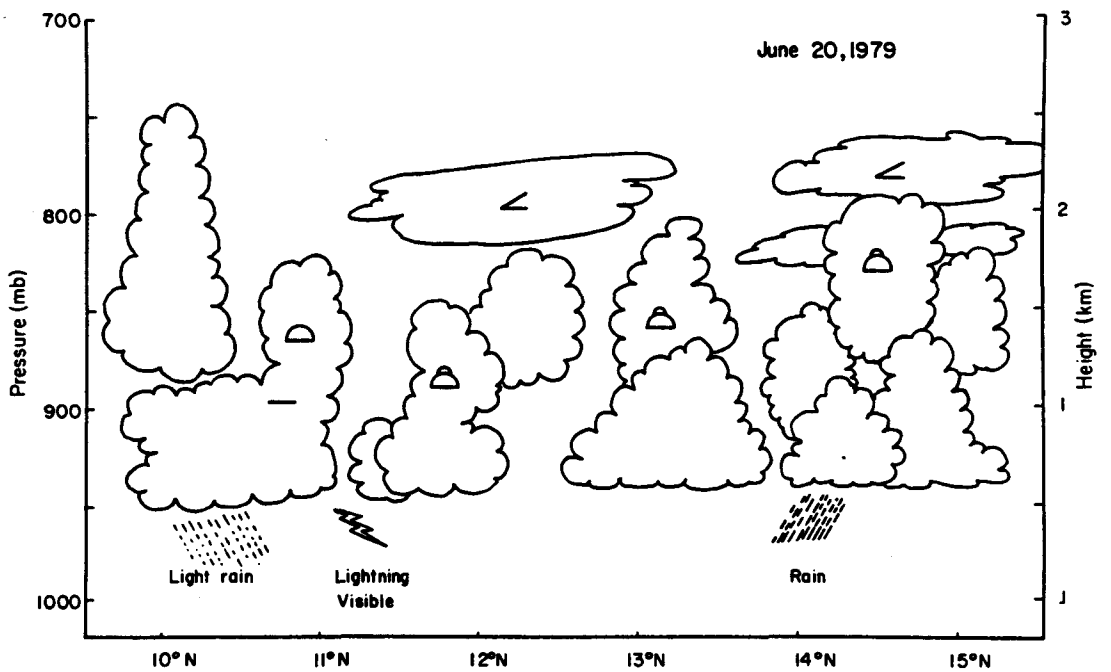

Fig. 7. Cross-section of cloud structure along flight of NCAR Electra on June 20, 1979 obtained from aircraft observer's reports and satellite photos. Note the layered clouds in the Southern Arabian sea region (10° N) versus the isolated cumulus and cumulonimbus in the Northern Arabian Sea region (15° N).

reports and 16 mm motion pictures taken from the aircraft. The results are shown in Figure 7, which indicate multiple layers of clouds, particularly stratocumulus (SC) and cumulus (CU). Several researchers have used θ_v, the virtual potential temperature, to identify the mixed and cloud layers in the tropical boundary layer (e.g., LeMone, 1980; Rao and Haney, 1982). Profiles of mean values of virtual potential temperature θ_v, equivalent potential temperature θ_E and wind speed for the Southern Arabian Sea region on June 20, 1979 are given in Figure 9. Profiles are fitted by eye. The mean θ_v profile shows a stable layer from near the surface (100 m) to approximately 1 km (900 mb) indicating little convective mixing in the lower levels. A strong, capping stable layer is evident from approximately 900 to 700 mb. θ_E is included because it is an important parameter in the boundary layer due to the conditionally unstable nature of the mean tropical atmosphere (Holton, 1979). The mean vertical profile of θ_E indicates a shallow conditionally stable layer extending from 100 m to about 700 m above the surface. Thus, both θ_v and θ_E show increasing values with height up to about 700 m indicating an absolutely stable stratification over the Southern Arabian Sea region.

The mean resultant wind speed profile over the Southern Arabian Sea supports the conclusions drawn from the θ_v and θ_E profiles. The height of the maximum wind speed, approximately 1 km, agrees roughly with the height of the strong capping stable layer. There appears to be strong shear in the wind profile up to a height of about 700 m which was the height of the stable layer in the θ_E profile.

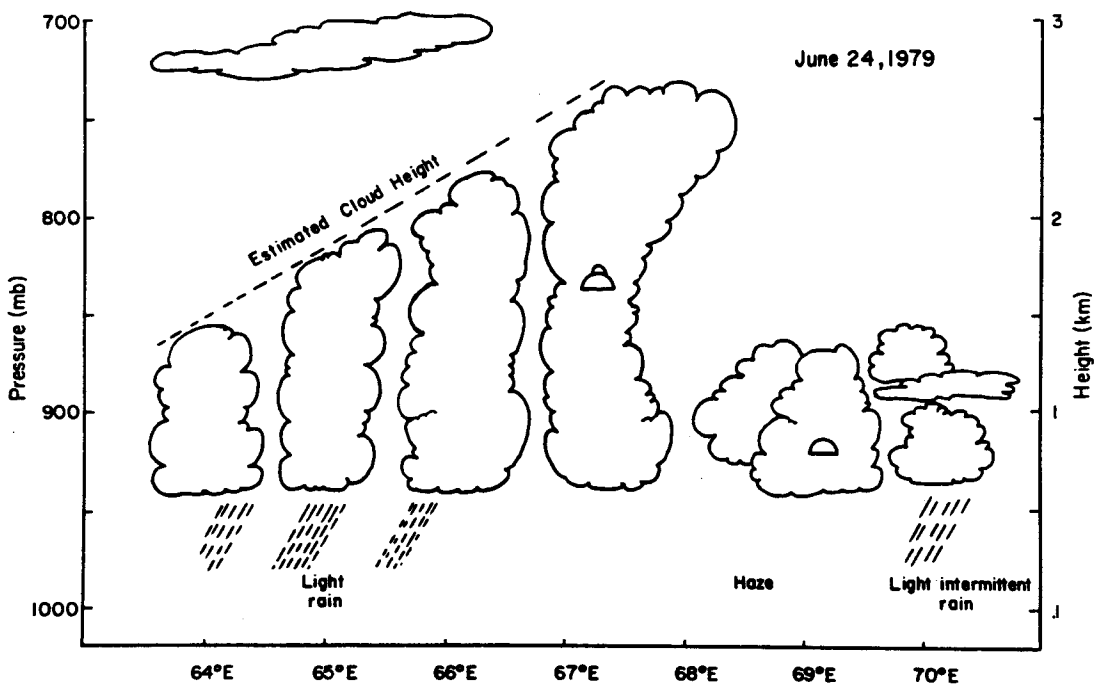

Fig. 8. Cross-section of cloud structure for June 24, 1979 similar to Figure 7. Note the cumulus congestus located at approximately 67.5° E along the flight track. Convective activity is suppressed east of the congestus region (69° E to 70° E).

5.1.1.2. *Northern Arabian Sea.* Mean profiles of θ_v, θ_E and wind speed for the Northern Arabian Sea on June 20 are given in Figure 10. The mean θ_v profile exhibits a well mixed near-neutral layer from 100 to 800 m (920 mb) with a strong capping layer aloft. The mean θ_E profile indicates strong convectively unstable conditions throughout the monsoon boundary layer. Synoptic conditions, again obtained from Electra's 16 mm

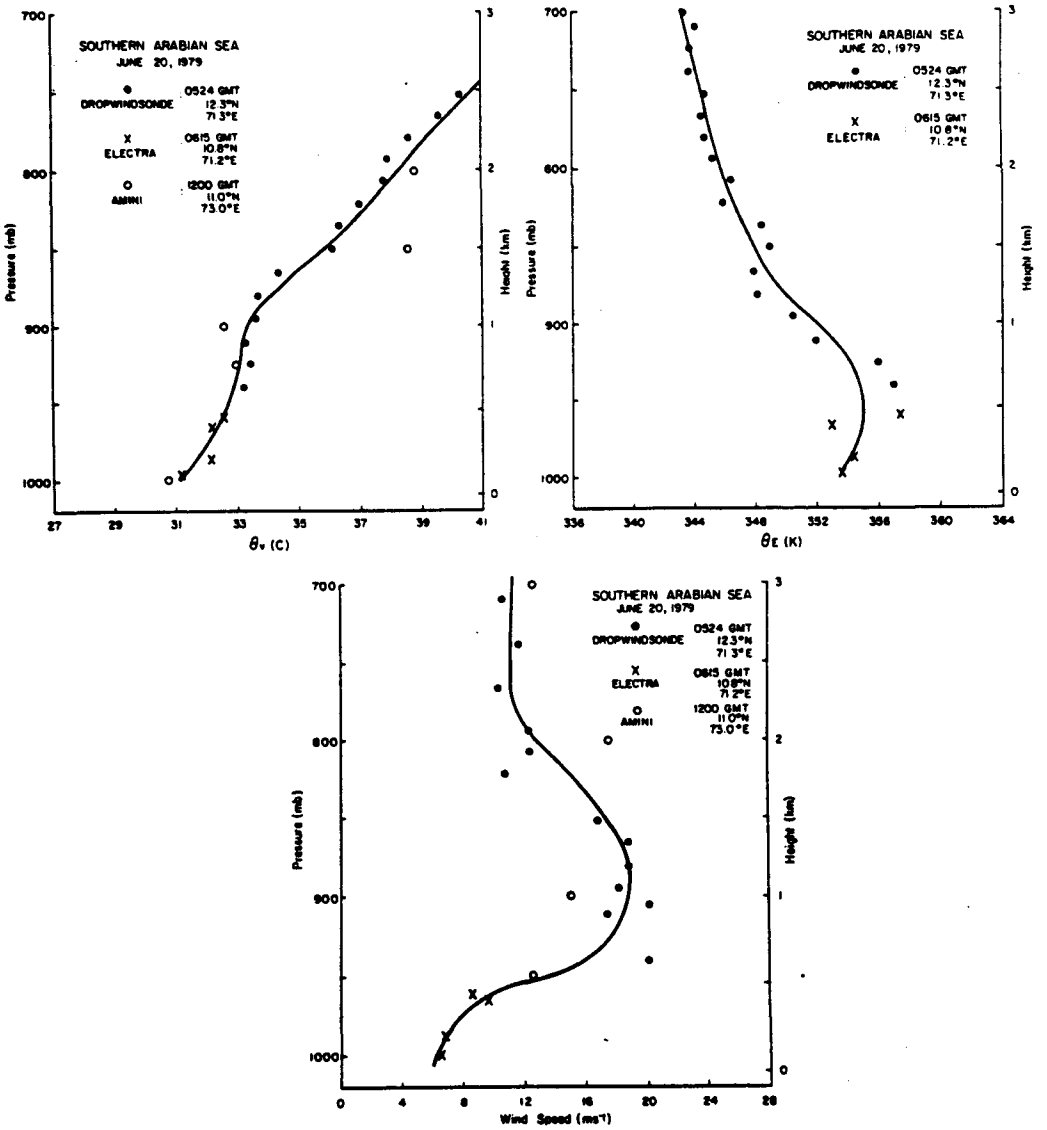

Fig. 9. Vertical profiles of mean virtual potential temperature θ_v, mean equivalent potential temperature θ_E and mean resultant wind speed for the Southern Arabian Sea for June 20, 1979. Data are from the Indian ship AMINI, NCAR Electra low-level observations and dropwindsondes. Note the positive values of $\partial\theta_v/\partial z$ and $\partial\theta_E/\partial z$ in the lowest 700 m indicating absolutely stable stratification. The jet core height agrees well with the height of the capping stable layer.

movies and the observer's reports indicate cumulus cloud systems in this region with cloud bases at approximately 940 mb (Figure 7). Thus, differences in cloud type and amount in the two regions on June 20 are evident in the thermodynamic profiles. The stratocumulus and layered cumulus evident in the Southern region (10° N) of Figure 7 are associated with an absolutely stable stratification in the subcloud layer. Cumulus and even towering cumulus of the Northern region (15° N) are generally associated with a well-mixed subcloud layer.

The mean resultant wind speed profile over the Northern Arabian Sea indicates a jet depressed in height with a maximum mean resultant wind speed of about 22 m s^{-1} at a height of 700 m (930 mb). Observations of a strong convectively unstable boundary layer from the θ_E profile and a well-mixed subcloud layer up to approximately 800 m with a strong stable layer aloft from the θ_v profile support the observed mean wind profile. Thus it can be inferred that the mean vertical structure of the jet is not uniform over the Arabian Sea during the monsoon period.

5.1.2. JUNE 24

5.1.2.1. *Western Arabian Sea.* Synoptic conditions over the Western Arabian Sea consisted of isolated cumulus cloud systems with generally stronger winds than over the Eastern Arabian Sea region (Figure 8). Mean profiles of θ_v, θ_E and wind speed similar to Figure 10 are given in Figure 11 for the Western Arabian Sea on June 24. The mean θ_v profile exhibits a near-neutral profile up to approximately 800 m (920 mb) suggesting considerable mixing in the subcloud layer. A strong, capping stable layer is evident aloft between 920 and 700 mb. The mean profile of θ_E shows a very weak conditionally unstable layer from near the surface to 700 mb. The scatter in lower layers could be due to the dropwindsonde observations obtained from two different locations.

The mean resultant wind speed over the Western Arabian Sea for June 24 indicates a jet depressed in height similar to that over the Northern Arabian Sea on June 20. The temperature profiles and the stability characteristics discussed above are consistent with the wind profile.

5.1.2.2. *Eastern Arabian Sea.* The synoptic-scale thermodynamic setting over the Eastern Arabian Sea on June 24 consisted of generally suppressed conditions west of an extensive cloud system located at approximately 16° N, 71° E. Mean profiles of θ_v, θ_E and wind speed for the Eastern region are given in Figure 12. The mean θ_v profile shows two interesting features: (i) the mixed layer extends only to approximately 600 m (940 mb) versus 1 km (900 mb) over the Western Arabian Sea and (ii) the strong, capping stable layer is not evident until approximately 1.5 km (850 mb) with a near-neutral layer between 600–1500 m (940–850 mb), suggesting the existence of multiple cloud layers as opposed to the strong capping layer at 1 km over the Western Arabian Sea region. Aircraft observers' reports indicate the lowest cloud base at approximately 600 m (Figure 8).

The mean θ_E profile shows a weak unstable layer from near the surface up to 1 km (900 mb). The presence of the strong convectively unstable layer from approximately

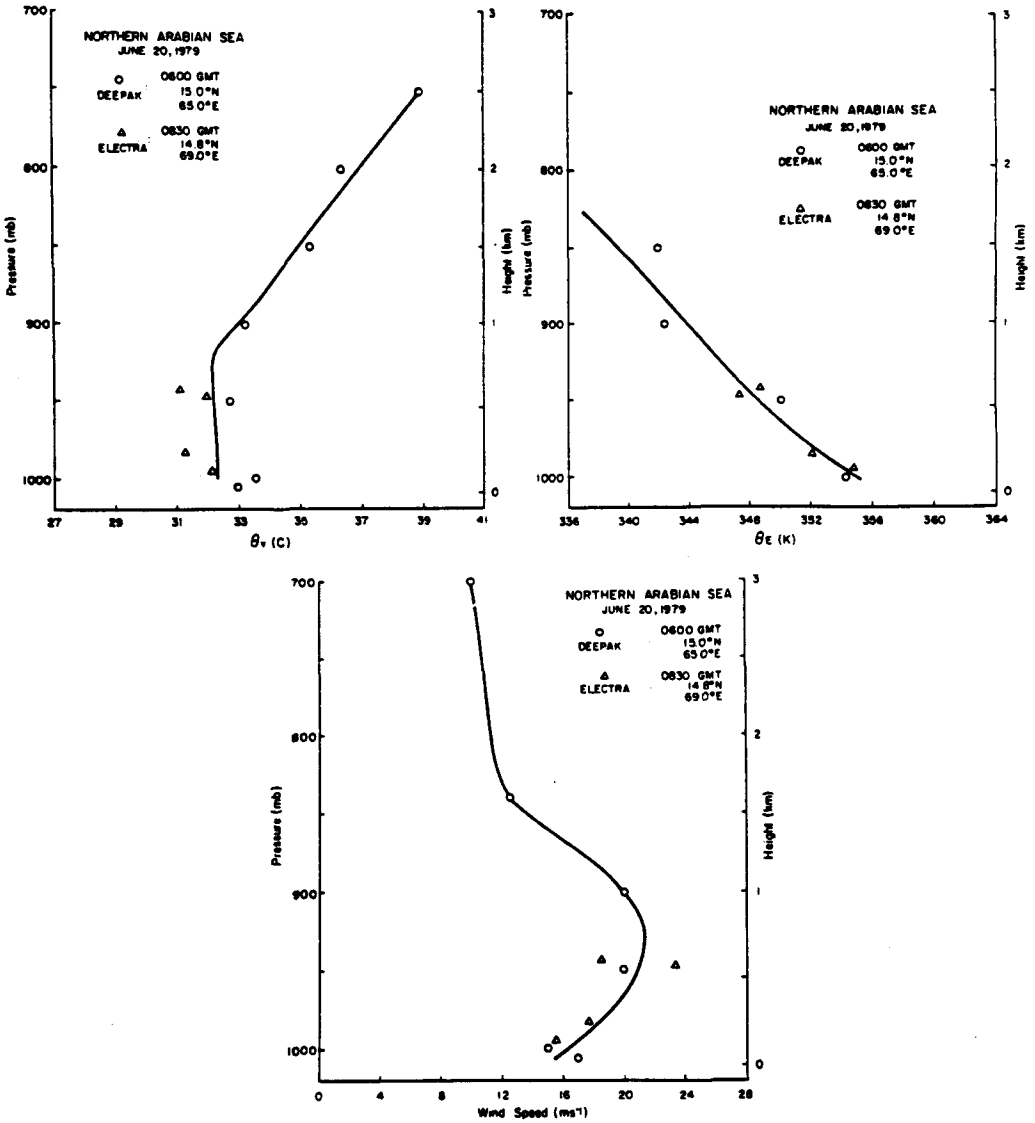

Fig. 10. Vertical profiles similar to Figure 9, except for Northern Arabian Sea on June 20, 1979. Data are from Indian ship DEEPAK and low-level Electra observations. The near-neutral mixed layer extending to approximately 800 m (920 mb) evident in the θ_v profile agrees roughly with the height of the jet core. Note however the depressed height of the core.

900 to 880 mb agrees with the observations of multiple cloud layers, particularly cumulus and stratocumulus. The wind speed profile of Figure 12 shows a very deep, flat jet extending to a height of about 1600 m (840 mb) over the Eastern Arabian Sea. Again, this structure is consistent with temperature and stability data. Grossman and Durran (1984) used the June 24 boundary-layer mission as a case study for offshore convection and noted that the downstream profile (Eastern Arabian Sea region) was taken just west

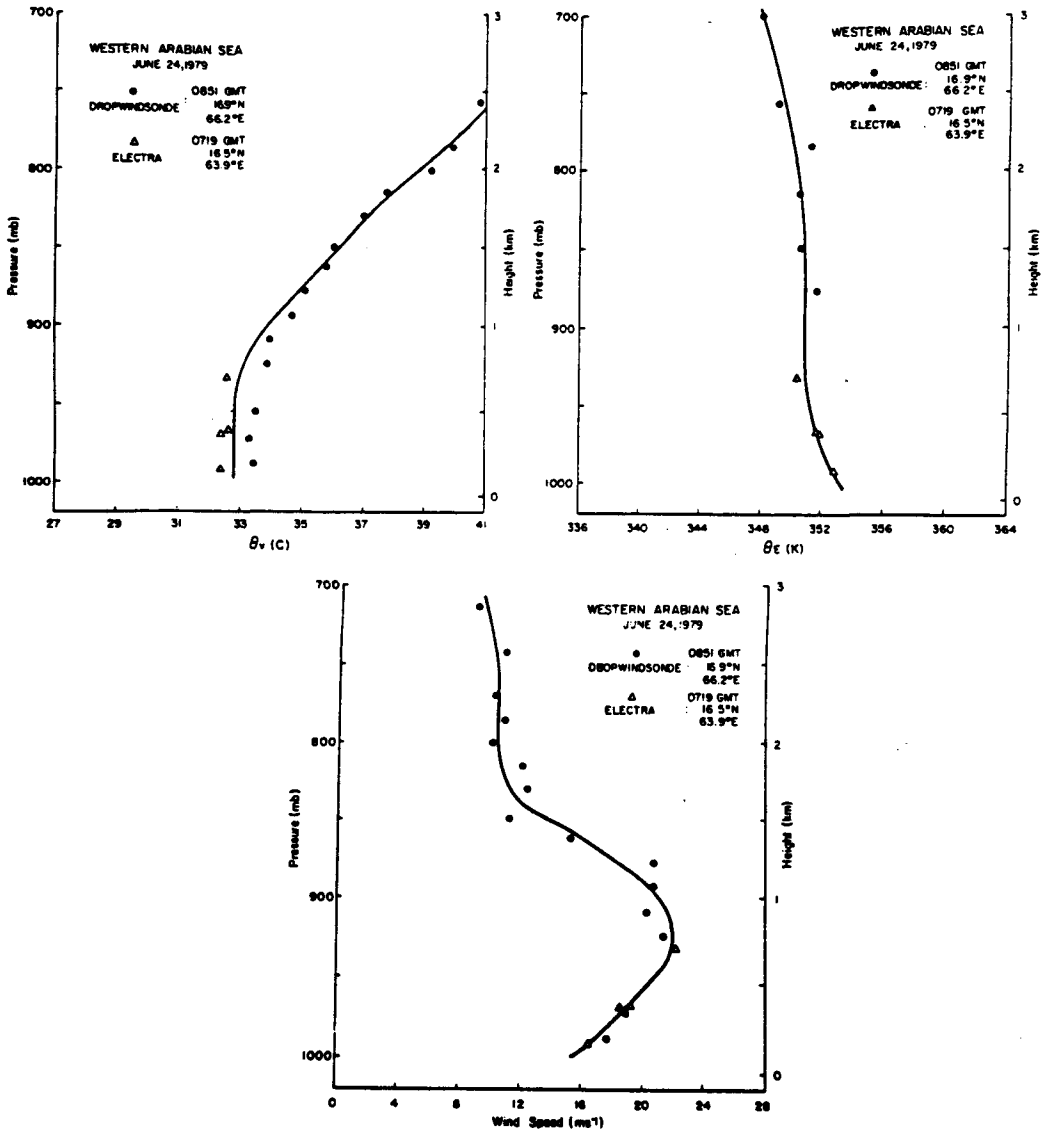

Fig. 11. Vertical profiles as in Figure 9, except for the Western Arabian Sea region on June 24, 1979. Data are from dropwindsonde and low-level Electra observations only. Note the similarity to Figure 10 in that both show the height of the jet situated roughly at the height of the strong capping inversion.

of an area of cumulonimbus and that as the flight progressed westward, convective activity was very suppressed. There was a cirrus shield extending away from offshore convection over Western India with a lack of intense convective activity until approximately 440 km offshore (67.5° E) where a cumulus congestus area was located. Grossman and Durran (1984) hypothesize that the general suppression of convective activity east of the cumulus congestus area (Figure 8) was due to downward motion under the anvil cloud. Low-level (up to about 400 m) estimates of vertical velocity by

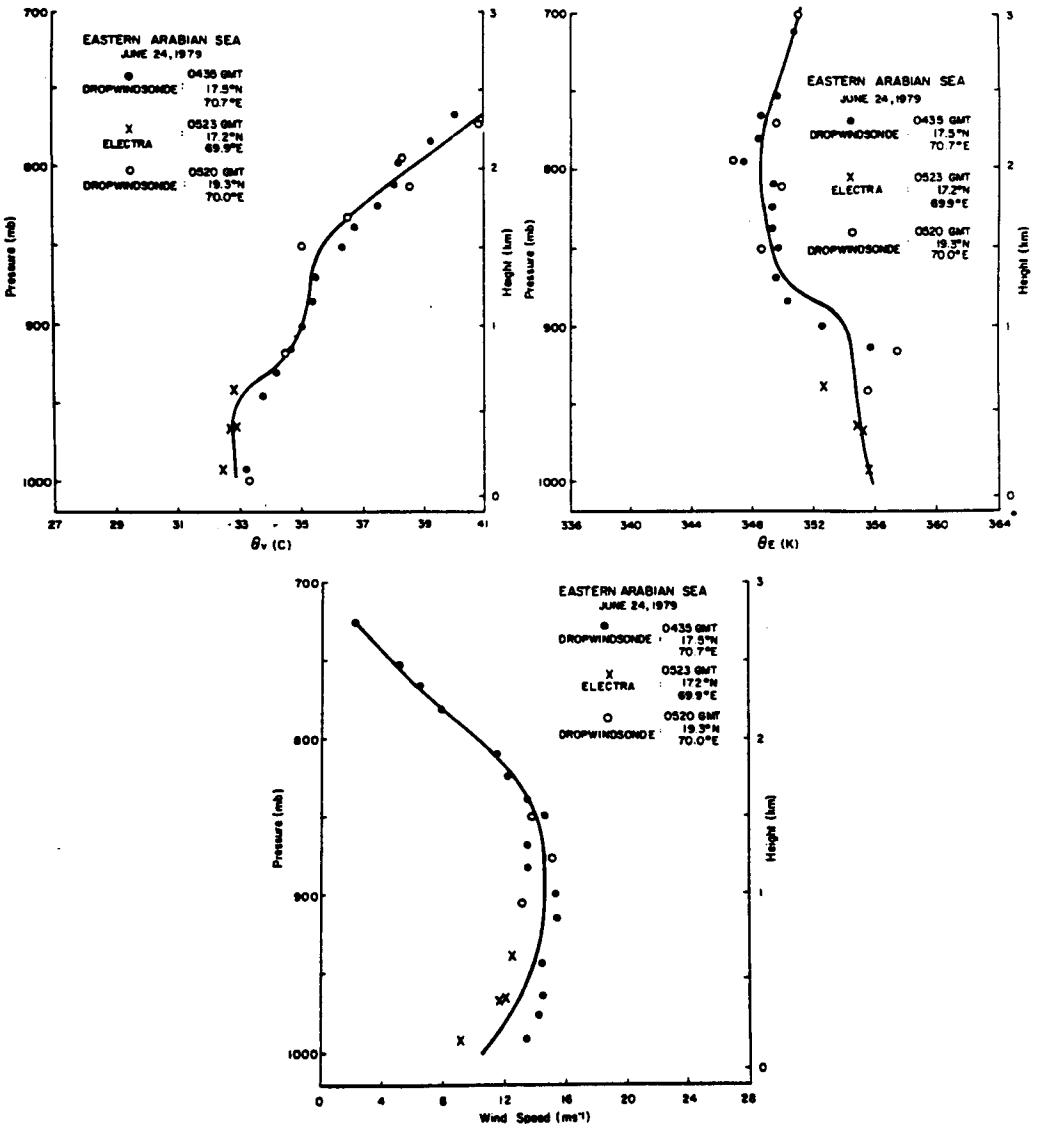

Fig. 12. Vertical profiles as in Figure 9, except for the Eastern Arabian Sea on June 24, 1979. Dropwindsonde and Electra data are used. The presence of multiple cloud layers is evident in both the θ_v and θ_E profiles. Note the shallow mixed layer (600 m) in the θ_v profile, but the strong stable layer is not evident until 1.5 km. The wind speed profile shows a very broad jet up to 1.6 km.

Grossman and Durran (1984) over the Eastern Arabian Sea area give values of approximately 3 cm s^{-1}, supporting the low-level well-mixed layer seen in the θ_v profile (Figure 12).

5.2 Balance of Forces along Mean Trajectory

Computations of forces along a mean trajectory were carried out for June 24, 1979 over the Arabian Sea in order to understand the balance of these forces in the monsoon

boundary layer. Under the assumption of mean horizontal flow with homogeneous turbulence, the equations of motion may be written as:

$$\frac{d\overline{V}_s}{dt} + f(\overline{V}_{gn} - \overline{V}_n) = \frac{1}{\overline{\rho}} \frac{\partial \overline{\tau}_s}{\partial z}$$

$$\frac{d\overline{V}_n}{dt} - f(\overline{V}_{gs} - \overline{V}_s) = \frac{1}{\overline{\rho}} \frac{\partial \overline{\tau}_n}{\partial z} \tag{1}$$

where 's' and 'n' refer to components parallel and perpendicular to the surface wind, $\tau = (\tau_s, \tau_n)$ represents the wind stress, $V_g = (V_{gs}, V_{gn})$ represents the geostrophic wind and overbars denote ensemble averages.

For June 24, the flight track was approximately into the mean surface trajectory within $\pm$ 10 deg. Thus lateral and longitudinal gusts measured by the NCAR Electra aircraft can be used as an approximation to the tangential and normal components 's' and 'n'. Mean winds $\overline{V}_s$ and $\overline{V}_n$ were obtained by averaging over each run for the specified height. Dropwindsonde data over the region of the flight tracks provided mean surface pressure data at 990 mb. Components of the geostrophic wind, normal component V_{gn} and tangential component V_{gs}, were obtained from both dropwindsonde data and an analysis of geostationary satellite data at approximately 900 mb and were assumed constant with height. The analysis of geostationary satellite data was similar to that used by Stout and Young (1983) in that cloud wind level was assumed to be near that of the maximum lower tropospheric wind (Findlater, 1969). Stout and Young (1983) used the 900 mb level representative of the geostrophic flow.

The Lagrangian acceleration term $d\overline{V}_s/dt$ along a streamline with the s direction positive downstream and the n direction positive to the right was approximated from:

$$\frac{d\overline{V}_s}{dt} = \frac{\partial \overline{V}_s}{\partial t} + \overline{V}_s \frac{\partial \overline{V}_s}{\partial s} + \overline{w} \frac{\partial \overline{V}_s}{\partial z} \tag{2}$$

where $\overline{w}$ is the vertical velocity and partial derivatives $\partial/\partial t$, $\partial/\partial s$, and $\partial/\partial z$ are local change, variation along the streamline and vertical change, respectively. Analysis of surface data from the Indian ships DEEPAK (June 23 1800 GMT – June 25 1800 GMT) and DARSHAK (June 24 0600 GMT – June 25 1800 GMT) located in the MONEX observation area revealed almost constant wind speeds and direction (DEEPAK 15 m s^{-1}, 250–270°; DARSHAK 10 m s^{-1}, 250–270°) for this time period. Thus, quasi-stationarity ($\partial \overline{V}_s/\partial t \approx 0$) can be assumed. Assuming no cross-stream gradients ($\partial/\partial n = 0$), the vertical velocity $\overline{w}$ can be estimated from the two-dimensional divergence equation integrated over a depth z as:

$$\overline{w} = -\int_0^z \operatorname{div} \mathbf{V}\, dz \approx -\frac{\Delta u}{\Delta s} z \tag{3}$$

where $\operatorname{div} \mathbf{V} \approx \Delta u/\Delta s$.

Values for the gradient of the wind stress $\bar{\tau}_s$, approximated by the eddy-correlation method, were obtained from the stress profiles and a centered finite-difference scheme. Extension to the surface for the stress (friction) term was obtained by using the drag coefficient formulation given by Large and Pond (1981):

$$\tau = \rho\,[0.49 + 0.065\,U_{10}] \times 10^{-3}\,U_{10}^2 \tag{4}$$

where U_{10} is the wind speed at 10 m.

Plots of the vertical variation of the various forces for June 24 over the Western and Eastern Arabian Sea regions are shown in Figures 13 and 14, respectively. Analysis of the balance of forces for June 20 over the Arabian Sea was not possible due to the fact that the flight track was not along the boundary-layer wind. Values of the different forces were calculated at three altitudes: 180, 385 and 680 m. Extrapolated values near the surface for the geostrophic departure and Lagrangian acceleration terms are denoted by dotted lines.

A feature common to both regions, Western and Eastern Arabian Sea, is that as expected, the friction and advective acceleration terms generally dominate in the lowest 200 m with the geostrophic departure an order of magnitude smaller. The Western Arabian Sea region (Figure 13), characterized by isolated cumulus activity with a

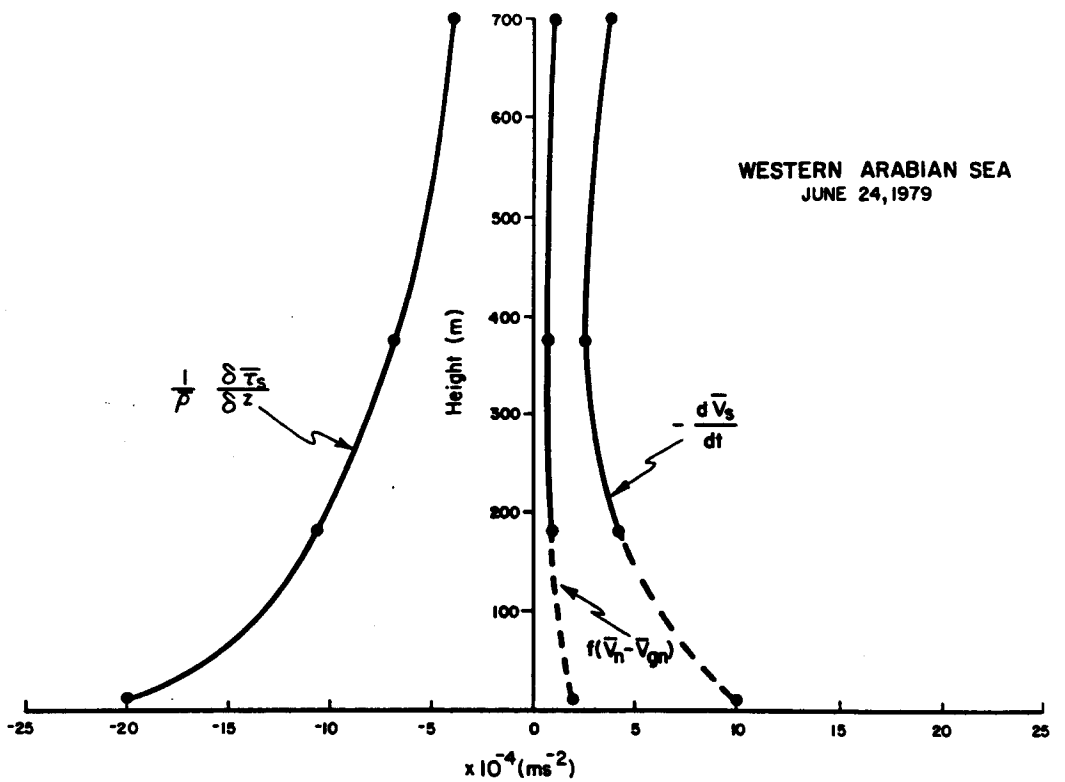

Fig. 13. Balance of forces for June 24, 1979 Western Arabian Sea region showing the vertical variation of geostrophic departure ($f(\bar{V}_n - \bar{V}_{gn})$), acceleration ($d\bar{V}_s/dt$) and friction $\left(\frac{1}{\bar{\rho}}\,[\partial\bar{\tau}_s/\partial z]\right)$.

well-mixed layer up to 1 km and generally stronger, more constant winds than over the Eastern Arabian Sea region, shows a dominance by the friction term due primarily to the stronger winds. However, the advective acceleration term $d\bar{V}_s/dt$ is generally not as large over the Western Arabian Sea as over the Eastern Arabian Sea. We hypothesize that this may be due to two factors: (i) the weaker mean vertical velocities $\bar{w}$ over the Western Arabian Sea region in the lowest 600 m. Values estimated from Equation (3) are on the order of 0.1 to 0.3 cm s^{-1} as opposed to 1–2 cm s^{-1} over the Eastern Arabian Sea. The stronger $\bar{w}$ values over the Eastern region are believed to be due to the low-level upward motion under the anvil cloud associated with the large synoptic system mentioned earlier (Grossman and Durran, 1984); (ii) the stronger, more constant winds over the Western Arabian Sea region in the lowest 600 m. The wind profile (Figure 11) obtained from aircraft, ship and dropwindsonde data in the Western Arabian Sea shows little variation over a 2.5° × 2.5° latitude region centered at 16.5° N, 63.9° E. Thus $\Delta u/\Delta s$ is small (order of magnitude 7×10^{-6} s^{-1}). Variations of $\Delta u/\Delta s$ over the Eastern Arabian Sea region in which the wind profile shows a weaker jet are approximately two to three times larger.

Krishnamurti *et al.* (1983) studied the monsoon flow over the Arabian Sea using a three-dimensional numerical model. The model uses *K*-theory assumptions for the

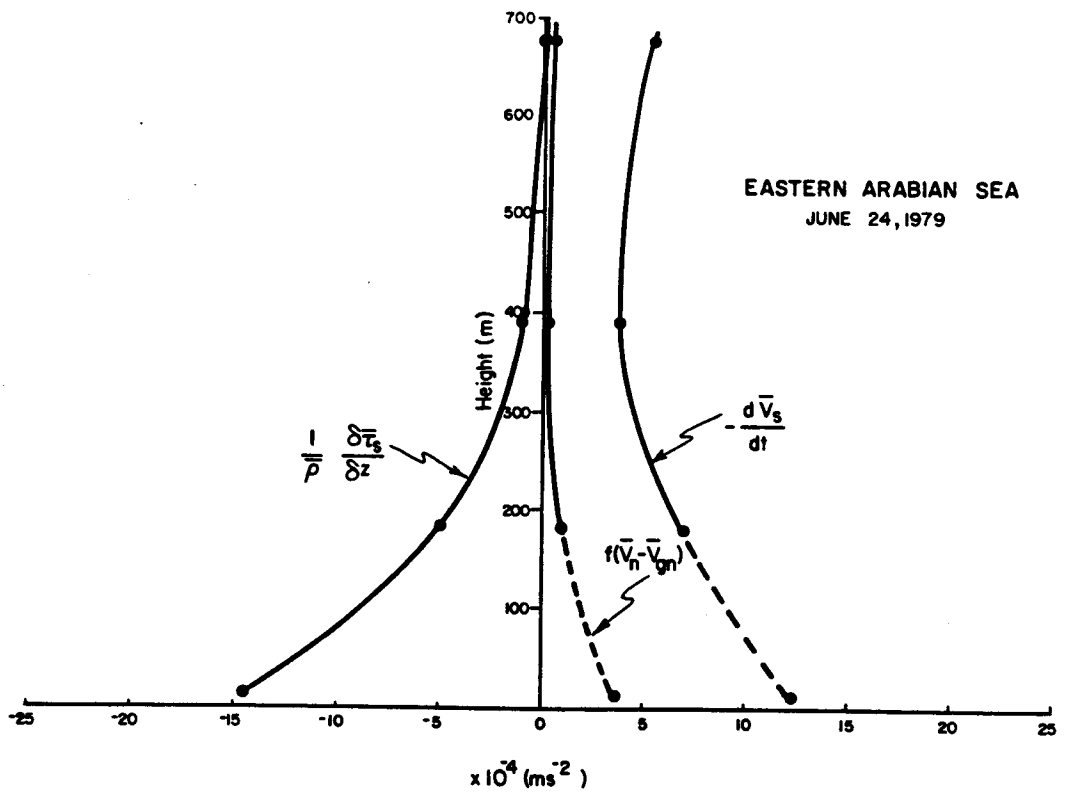

Fig. 14. Balance of forces similar to Figure 13 except over the Eastern Arabian Sea for June 24, 1979.

boundary layer and prescribes three-dimensional pressure patterns. North of 10° N over the Arabian Sea at the 0.2 km level, Krishnamurti *et al.* (1983) observed that the Coriolis force, pressure gradient and frictional forces balanced, with horizontal advective acceleration playing only a minor role. Estimates of the geostrophic departure term, $f(\overline{V}_n - \overline{V}_{gn})$ from the results of this numerical model indicated that it was generally smaller than the friction term but approximately of the same order of magnitude as the advective acceleration term. Observations (Figures 13 and 14) for June 24 however, indicate a relative dominance of advective acceleration over geostrophic departure at the 0.2 km level. This could be due to some of the simplifying assumptions such as K theory in the model.

Reverdin and Sommeria (1983) used constant-level balloons at approximately 900 mb to study the balance of forces over the Arabian Sea. Trajectories were divided into pre-monsoon (May 15 to June 11) and monsoon (June 12 to July 8) periods. Their results were average values over several days. They found the friction and Lagrangian acceleration terms to be of the order of 3×10^{-4} (m s^{-2}) and the geostrophic departure term to be about 1×10^{-4} (m s^{-2}). These values agree well with our results (Figures 13 and 14). Stout and Young (1983) studied forces along trajectories across the Arabian Sea using satellite-derived winds averaged over part of the monsoon period of about 1.5 months. Their values at 900 mb indicated similar results with reference to the balance of forces.

The balance of forces in the trade wind boundary layer observed over the tropical oceans is markedly different from the balance presented here for the monsoon boundary layer. Results from ATEX (Brümmer, 1976) and BOMEX (Holland and Rasmusson, 1973) indicate that the acceleration term ($d\overline{V}_s/dt$) is generally negligible over tropical oceans in the trade wind zone as compared to the friction ($1/\overline{\rho}\,[\partial\overline{\tau}_s/\partial z]$) and geostrophic departure ($f(\overline{V}_n - \overline{V}_{gn})$) terms. However, for the present results over the Arabian Sea (Figures 13 and 14), the acceleration term is a dominant term in the lowest 300 m with an order of magnitude of about 10^{-3} (m s^{-2}). Over trade wind tropical oceans, it was found to be approximately of the order of 10^{-5} (m s^{-2}).

The balance in the lowest 300 m over tropical oceans is generally found to be between the geostrophic departure term and friction with surface values of the order of 10^{-4} (m s^{-2}). In contrast, all three terms make a significant contribution to the balance of forces in the lowest 300 m over the Arabian Sea for June 24. Friction and acceleration tend to be the dominant terms in the monsoon boundary layer but the geostrophic departure term is also significant. Near surface values for friction and acceleration are of the order of 10^{-3} (m s^{-1}) and geostrophic departure of the order of 10^{-4} (m s^{-2}). A summary of the order of magnitude for various terms for trade-wind and monsoon boundary layers is given in Table I. The difference in the values between trade-wind and monsoon boundary layers is probably due to the basic difference in the large-scale mechanisms that produce the flow.

As seen in Table I, there is an imbalance in the comparison of forces along a trajectory. An average value of about 30×10^{-5} (m s^{-2}) on the same order of magnitude as the other forces, is observed for the imbalance in the monsoon boundary

TABLE I

Comparison of the forces ($m\ s^{-2}$) along a trajectory for Trade Wind and Monsoon Boundary Layers near the ocean surface

	Friction ($\times 10^{-5}$)	Geostrophic Departure ($\times 10^{-5}$)	Advective Acceleration ($\times 10^{-5}$)
Trade Wind (Typical)			
180 m	12	10	1
385 m	8	8	1
680 m	5	5	1
Monsoon			
Western Arabian Sea (*June* 24, 1979)			
180 m	100	10	50
385 m	70	10	30
685 m	40	10	30
Eastern Arabian Sea (June 24, 1979)			
180 m	50	10	70
385 m	20	10	50
680 m	10	10	50

layer. In a typical trade-wind boundary layer in which the magnitude of forces is generally one order of magnitude smaller than the monsoon boundary layer, the imbalance is approximately one order of magnitude smaller, on the order of 1×10^{-5} ($m\ s^{-2}$). Assumptions of a constant geostrophic wind with height in the monsoon layer along with no cross-stream gradients obviously contribute to the imbalance. A preliminary analysis of turbulent quantities of temperature, humidity and wind components also indicates that the assumption of homogeneous turbulence could be a contributing factor to the imbalance. It is interesting to note that the imbalance decreases from larger values near the surface approaching zero near the top of the boundary layer over the Western Arabian Sea but generally increases from the surface to the top of the boundary layer over the Eastern region.

5.3. A FREE JET-SURFACE LAYER MODEL FOR THE STRUCTURE OF THE EAJ

As discussed before, EAJ is a large scale phenomenon due to the combined effects of cross-equatorial flow and the mountains along the East African coast. Maximum wind speed in this jet has been observed to be at an altitude of about 1000 m over the Arabian Sea. The structure of the jet can thus be approximated by that of a 'free jet'. A simple model similar to the one derived by Reichardt and quoted by Schlichting (1979) was used to calculate the profile of the EAJ. This relationship is based on experimental finding that the distribution of excess momentum in the jet approximates a Gaussian distribution over the width of the jet. His relationship for the distribution of velocity u

and temperature T is given by:

$$\frac{T}{T_{max}} = \left[\frac{u}{u_{max}}\right]^{A_u/A_T} \tag{5}$$

where the subscript max refers to the maximum values and the scales for u and T must be arranged so that the points for which $u = 0$ and $T = 0$ are coincident. A_u and A_T are the Austausch coefficients for momentum and heat transfers, respectively. Businger *et al.* (1971) give a 'neutral' value of 1.35 for A_T/A_u so that:

$$\frac{T}{T_{max}} = \left[\frac{u}{u_{max}}\right]^{0.74} \tag{6}$$

Using a Gaussian type of distribution for the excess momentum in the jet,

$$\frac{u}{u_{max}} = \exp\left[-\frac{1}{2}\eta^2\right] \tag{7}$$

where $\eta = z/d$ with d = depth of the jet taken to be equal to the depth where $(u/u_{max})^2 = 0.368$. However, requiring that the depth of the jet be known dictates a partial knowledge of the structure of the jet itself. In essence, this structure is what is being diagnosed and is an unknown. A simple but somewhat crude way of approximating the depth of the jet is to take the 900 mb level (1 km) as the level of maximum winds, and assume the height of the surface layer z_s to be about 100 m over the ocean during strong wind conditions. Subtracting the two heights, a rough value of 900 m is obtained for the jet depth d. Figure 15 shows the vertical profile of wind speed using this formulation (Equation (7)) for the four observations regions. The solid line is the observed jet structure. The open circles indicate the profile obtained when the actual observed depth and u_{max} values are used in Equation (7). In all four cases, the model approximates the observed jet structure better near the core where the jet is more a 'free jet' and is affected less by the surface.

The obvious advantage of this model is its simplicity in that only satellite-derived winds at approximately 900 mb are needed to calculate the jet structure. The disadvantage is that this level might not always be the level of maximum winds and errors can result. Also, surface effects not taken into account are very important in determining the jet structure in the lowest hundreds of meters. Stout and Young (1983) used the 900 mb level as representative of the geostrophic flow. Approximation of the geostrophic wind components by the 850 mb pressure field for June 24 over the East Arabian Sea yielded values similar to those obtained by Young *et al.* (1980) for the low-level wind field measured at 1000 GMT for June 24. However, analysis of dew point depression data from dropwindsondes indicated the 930 mb level to be a more reasonable approximation to the cloud level. Dropwindsonde data indicated the maximum winds to occur at this level (Figure 11). Results from Grossman and Durran (1984) show that the height of the lifting condensation level (LCL) varied only about $\pm$ 5 mb around 945 mb over

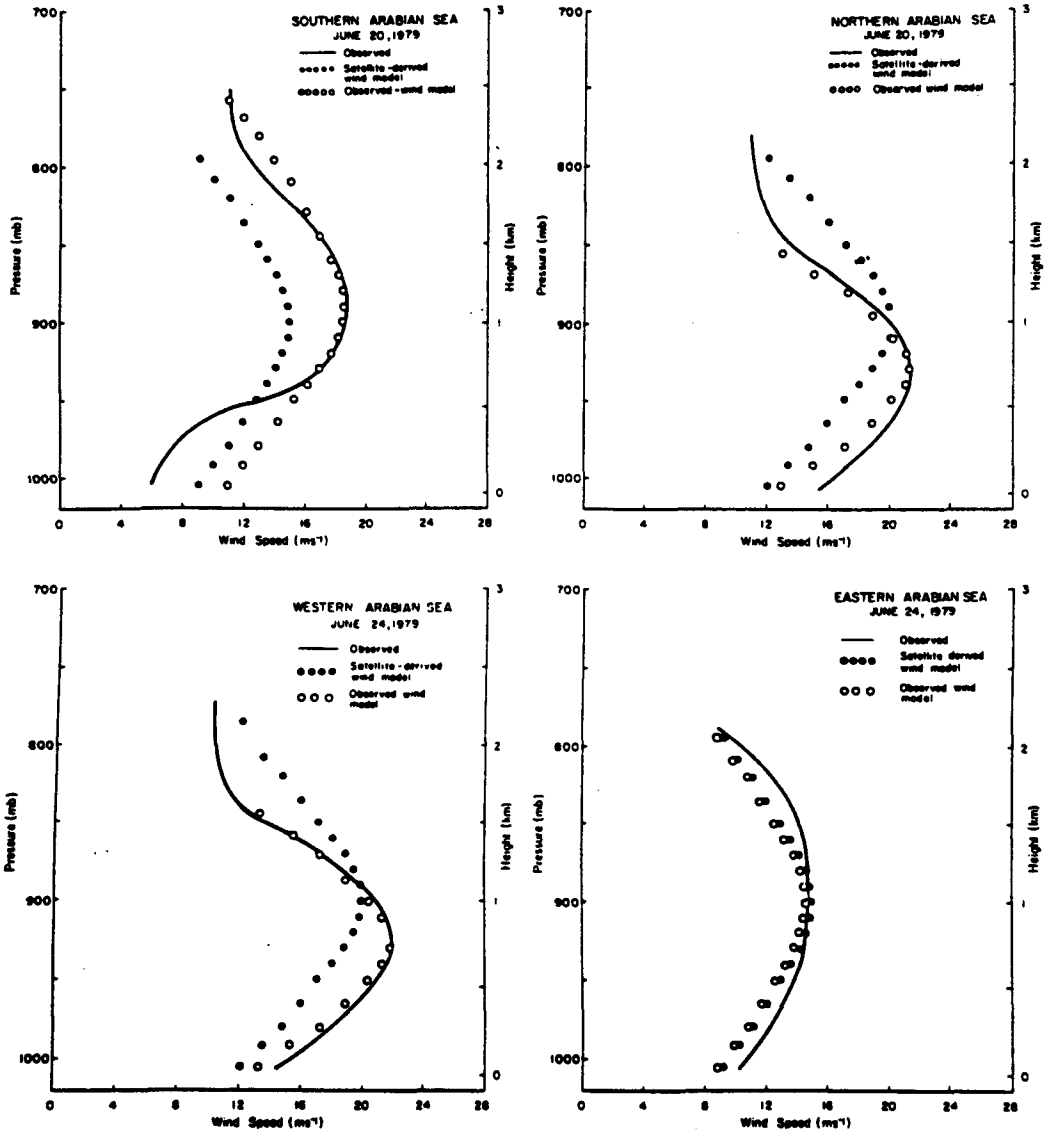

Fig. 15. Observed jet profiles versus the jet profiles calculated from the simple EAJ model for the four observation regions. The closed circles indicate the profile obtained using satellite-derived winds. The open circles indicate the profile obtained using the actual observed depth and u_{max} values.

the range of their flight mission suggesting that the cloud base and therefore the depth of the subcloud layer remained constant. For this specific case, use of the 900 mb winds as maximum as opposed to the 930 mb winds underestimates the geostrophic wind by approximately 2–3 m s^{-1} but more importantly displaces the jet core upward by approximately 300 m. Calculations of the jet profile from the model using 930 mb as the level of maximum winds better approximates the observed profile, indicating the effects of errors in the calculation of jet depth. Measurement errors in the satellite cloud winds

are generally of the order of 2 m s^{-1} (Hasler *et al.*, 1979). The maximum error in the model calculations of wind speed shown in Figure 15 is approximately 4 m s^{-1} with the exception of the lowest 300 m in the Southern Arabian Sea region on June 20. Considering the errors in satellite-derived winds and the simplicity of this model, errors of the order of 2–4 m s^{-1} are reasonable.

Comparison of the model results with the profiles observed by Pant and quoted by Long (1980), for ISMEX data over the Arabian Sea is shown in Figure 16. Also shown

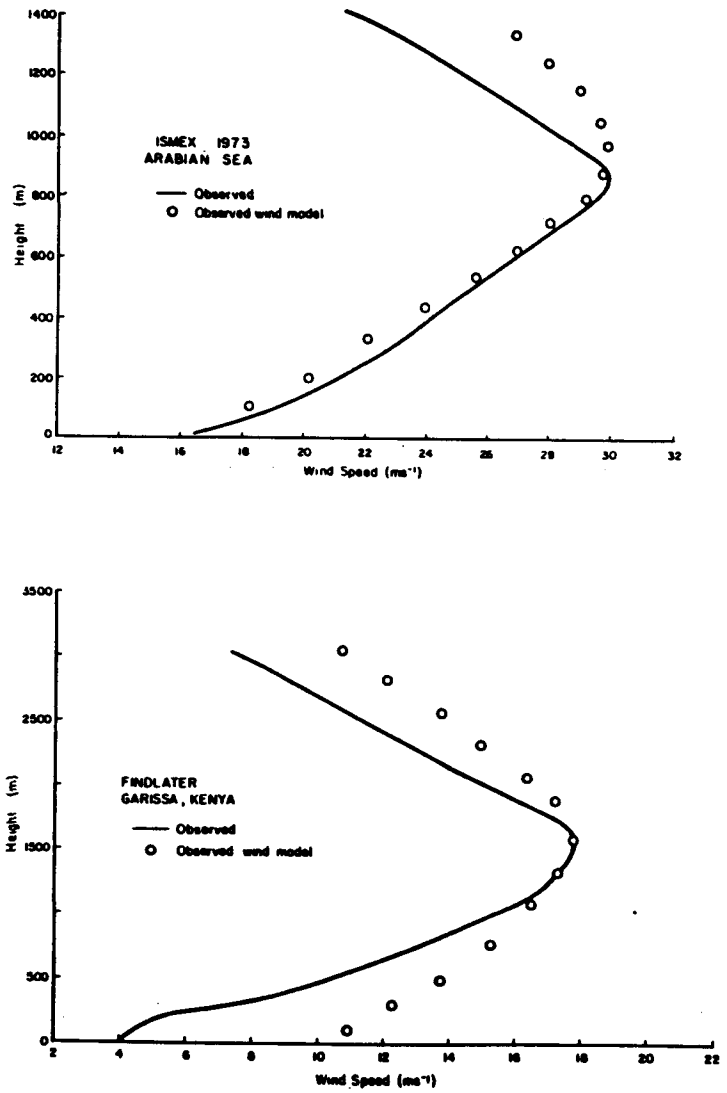

Fig. 16. Observed mean wind speed profiles versus EAJ model-calculated profiles using the ISMEX data base over the Arabian Sea 1973 (top) and for work by Findlater (1977b) over Garissa, Kenya (00°29′ S, 39°38′ E) (bottom). Observed profile over Garissa is an average of the mean southerly components from 0400–0700 GMT and 1000–1400 GMT for June and July 1973.

is a comparison with observations made by Findlater (1977b) over Garissa, Kenya (00° 29′ S, 39° 38′ E). The open circles indicate calculated values of wind speed using the actual observed depth and u_{max} values in Equation (7). Agreement between the model and observed profiles is good.

The overall accuracy of this simple model in approximating the structure of the EAJ depends on the assumptions that the 900 mb (1 km) level approximates the maximum wind level and that the surface layer is approximately 100 m during strong wind conditions. The observations seem to indicate that these assumptions are reasonable for conditions over the Arabian Sea.

6. Conclusions

Analysis of boundary-layer data obtained by NCAR Electra aircraft over the Arabian Sea during MONEX 79 in conjunction with synoptic, ship and dropwindsonde data revealed interesting non-homogeneous features of the monsoon boundary layer. Synoptic conditions in which there were multiple layers of clouds (June 20 Southern Arabian Sea and June 24 Eastern Arabian Sea) as seen in the virtual temperature structure were associated with a more elevated jet situated roughly at the height of the strong capping inversion layer. Locations in which there existed a more well-mixed layer near the surface up to 1 km (June 20 Northern Arabian Sea and June 24 Western Arabian Sea) were generally associated with more cumulus activity and showed a jet structure depressed in height. The thermal structure of the boundary layer thus seems to play an important role in the EAJ structure.

A free-jet model suggested here could be of help in operational short-range monsoon weather forecasting. This simple model estimates the mean wind structure of the EAJ reasonably well when given just satellite-derived winds at 900 mb. Winds near the surface estimated by this model can then be used in conjunction with bulk methods to calculate surfaces fluxes for use in weather forecasting models.

The mean structure of the monsoon boundary layer over the Arabian Sea appears to be markedly different from that of the trade-wind marine boundary layer in two aspects. One is the existence of a jet and the associated thermal structure of the boundary layer. Another is the existence of significant advective acceleration particularly in the lower levels of the marine boundary layer. One might expect that these variations in the mean structure caused by large-scale features would in turn affect the turbulence structure in the boundary layer.

A major limitation in the understanding of the monsoon boundary layer is the lack of observations. It will be of interest to investigate whether the pre-monsoon marine boundary-layer structure is the same as that of the trade-wind marine boundary layer. Variations in the structure and hence the processes of the boundary layer in the core of the EAJ as against regions of the Arabian Sea where EAJ does not exist will be another area of interest. Further coordinated observations are certainly needed to improve our understanding of the monsoon boundary layer.

Acknowledgements

The work was supported by the Global Atmospheric Research Program of the National Science Foundation under the Grant ATM–82–17960.

References

Bannon, P. R.: 1982, 'On the dynamics of the East African Jet. III: Arabian Sea Branch', *J. Atmos Sci.* **39**, 2267–2278.

Brümmer, B.: 1976, 'The Kinematics, Dynamics and Kinetic Energy Budget of the Trade Wind Flow over the Atlantic Ocean', *Meteor.-Forsch.-Ergeb.* **B11**, 1–24.

Businger, J. A., Wyngaard, J. C., Izumi, Y., and Bradley, E. F.: 1971, 'Flux Profile Relationships in the Atmospheric Surface Layer', *J. Atmos. Sci.* **18**, 181–189.

Findlater, J.: 1969, 'A Major Low Level Air Current near the Indian Ocean During the Northern Summer', *Quart. J. Roy. Meteorol. Soc.* **95**, 362–380.

Findlater, J.: 1977a, 'A Numerical Index to Monitor the Afro-Asian Monsoon During the Northern Summers', *Meteorol. Mag.* **106**, 170–180.

Findlater, J.: 1977b, 'Observational Aspects of the Low Level Cross Equatorial Jet Stream', T. N. Krishnamurti (ed.), in *Monsoon Dynamics*, Birkhauser Verlag, Basel, Stuttgart, pp. 1251–1262.

Grossman, R. L. and Durran, D. R.: 1984, 'Interaction of Low-level Flow with the Western Ghat Mountains and Offshore Convection in the Summer Monsoon', *Mon. Wea. Rev.* **112**, 652–672.

Hasler, A. F., Skillman, W. C., Shenk, W. E., and Steranka, J.: 1979, 'In situ Aircraft Verification of the Quality of Satellite Cloud Winds over Oceanic Regions', *J. Appl. Meteorol.* **18**, 1481–1489.

Holland, J. Z. and Rasmusson, E. M.: 1973, 'Measurements of the Atmospheric Mass, Energy and Momentum Budgets over a 500 km Square of the Tropical Ocean', *Mon. Wea. Rev.* **101**, 44–55.

Holton, J. R.: 1979, *An Introduction to Dynamic Meteorology*, Academic Press, N.Y., 319 pp.

Krishnamurti, T. N., Molinari, J., and Pan, H. L.: 1976, 'Numerical Simulation of the Somali Jet', *J. Atmos. Sci.* **33**, 2350–2362.

Krishnamurti, T. N., Wong, V., Hua-Lu Pan, Pasch, R., Molinari, J., and Ardanuy, P.: 1983, 'A Three-Dimensional Planetary Boundary Layer Model for the Somali Jet', *J. Atmos. Sci.* **40**, 894–908.

Large, W. G. and Pond, S.: 1981, 'Open Ocean Momentum Flux Measurements in Moderate to Strong Winds', *J. Phys. Oceanogr.* **11**, 324–336.

LeMone, M. A.: 1980, 'The Marine Boundary Layer', *Workshop on the Planetary Boundary Layer*, American Meteorological Society, Boston, MA, pp. 182–246.

Long, C. S.: 1980, 'Analysis of Aircraft Measurements of Boundary Layer Turbulence in Monsoonal Flow', Master's Thesis submitted to the University of Wisconsin-Madison, 93 pp.

Rao, G. V. and Haney, J. L.: 1982, 'Kinematic and Thermal Structures of Two Surges of Flow in the Northern Mozambique Channel Area', *Quart. J. Roy. Meteorol. Soc.* **108**, 957–974.

Reverdin, G. and Sommeria, G.: 1983, 'The Dynamical Structure of the Planetary Boundary Layer over the Arabian Sea, as Deduced from Constant-Level Balloon Trajectories', *J. Atmos. Sci.* **40**, 1435–1452.

Schlicting, H.: 1979, *Boundary-Layer Theory*, McGraw-Hill, 817 pp.

Sikka, D. R. and Grossman, B.: 1980, *Summer MONEX Chronological Weather Summary*, International MONEX Management Centre, New Delhi, India, December 1980 (first edition), pp. 49.

Stout, J. E. and Young, J. A.: 1983, 'Low-level Monsoon Dynamics Derived from Satellite Winds', *Mon. Wea. Rev.* **111**, 774–798.

Van de Boogaard, H.: 1977, 'The Mean Circulation of the Tropical and Subtropical Atmosphere – July'. NCAR Tech. Note NCAR/TN–118, 48 pp.

WMO: 1981, *The Summer MONEX Field Phase Report*, FGGE Operations Report, Vol. 8, World Meteorological Organization, Geneva.

Young, J. A., Virji, H., Wylie, D. P., and Lo, C.: 1980, *Summer Monsoon Wind sets from Geostationary Data*, Summer MONEX: 1 May – 31 July, 1979. NSF Report, Space Science and Engineering Center and Dept. Meteor., University of Winconsin-Madison, 127 pp.